Int J Fract
https://doi.org/10.1007/s10704-019-00376-8

ORIGINAL PAPER

A model for high temperature hydrogen attack in carbon steels under constrained void growth

Mohsen Dadfarnia · May L. Martin · David E. Moore · Steve E. Orwig · Petros Sofronis

Received: 17 April 2018 / Accepted: 5 June 2019

Abstract Petrochemical vessels exposed to high temperature and high pressure hydrogen gas may suffer from high temperature hydrogen attack (HTHA). HTHA is a hydrogen-induced degradation of carbon steels whereby internal hydrogen reacting with carbides forms methane gas bubbles, mainly on grain boundaries (GBs), with an associated loss in strength that can result in premature fracture of structural components. The design of equipment against HTHA is primarily based on the use of the empirical Nelson curves which are phenomenological and do not account for the underlying failure mechanisms and the material microstructure. Starting from the underlying deformation and fracture mechanisms, we present a simple constraint-based model for failure of steels by HTHA which involves growth of GB voids due to coupled diffusion of atoms along the GBs and creep of the matrix surrounding the voids. Since voids form only on some of the GBs, the uncavitated GBs geometrically constrain the growth of voids on the cavitated ones. The model is used to study void growth in HTHA of 21/4Cr–1Mo steel both in the presence and absence of externally applied stress. In the latter case, the model predictions are in good agreement with experimental results. Lastly, the model is used to develop a Nelson-curve type diagram in the presence of external stress in which the curves demarcating the safe/no-safe regimes are functions of the time to failure. This diagram though should be viewed as the result of the application of a new methodology toward devising mechanism-based Nelson curves and not as proposed new Nelson curves for the steel under investigation.

Keywords Hydrogen attack · Failure · Modelling · Carbon steels · Constrained void growth

D. E. Moore: Retired from BP Jan, 2017.

M. Dadfarnia (✉)· M. L. Martin · P. Sofronis
Department of Mechanical Science and Engineering, University of Illinois at Urbana-Champaign, 1206 West Green Street, Urbana, IL 61801, USA
M. Dadfarnia
e-mail: dadfarni@illinois.edu

M. Dadfarnia · M. L. Martin · P. Sofronis
International Institute for Carbon-Neutral Energy Research (WPI-I2CNER), Kyushu University, 744 Moto-oka, Nishi-ku, Fukuoka, Fukuoka 819-0395, Japan

M. Dadfarnia
Department of Mechanical Engineering, Seattle University, 901 12th Street, Seattle, WA 98122, USA

D. E. Moore · S. E. Orwig
Refining Technology and Engineering, BP Products North America, 150 West Warrenville Road, Naperville, IL 60563, USA

Present address:
M. L. Martin
Applied Chemicals and Materials Division, National Institute of Standards and Technology, 325 Broadway, Boulder, CO 80305, USA

Published online: 29 June 2019

1 Introduction

High temperature hydrogen attack (HTHA) still causes occasional failures in petroleum refinery and petrochemical plant equipment manufactured from carbon and low alloy steels, and is a continuing concern in the industry. The refining and petrochemical industries extensively use the American Petroleum Institute (API) Recommended Practice (RP) 941 (2016) to determine safe operating limits for steels under HTHA conditions. The API RP 941 standard consists of the "Nelson Curves" on a temperature/hydrogen gas partial pressure graph showing conditions under which HTHA can occur in different types of steels. The curves were designed completely phenomenologically and mainly drawn on the basis of empirical data from plant failures. The curves have gone through revisions and modifications as new failures were reported. A summary of the history of updating the Nelson curves can be found in the API Technical Report 941 (2008).

HTHA is a very complex mechanical-physical-chemical phenomenon. It involves H uptake from the surface, dissolution of carbides, diffusion of C and H to susceptible sites, reaction of C with H to create methane, and growth of voids due to the internal methane gas pressure and the applied load. Void growth can take place either by diffusion of atoms from the void surface (surface diffusion) into the grain boundary (GB) and away from the growing void along the grain boundary (GB diffusion) or by dislocation creep of the surrounding matrix.

A large number of researchers have studied the problem of void growth and have proposed models for HTHA. Shewmon (1976) proposed a void growth model under HTHA based on GB diffusion of iron. Sagues et al. (1978) developed an analytical model for the void growth mechanism considering both GB diffusion and power-law creep. Shih and Johnson (1982) followed the work of Sagues et al. (1978) by performing a more detailed study of the void growth in carbon steel. Sundararajan and Shewmon (1981) presented a model assuming only a fraction of GBs are cavitated. The uncavitated grains were assumed to impose a constraint on the void growth of the cavitated GBs (constrained cavitation growth) and as a result, the void growth is assumed to be accommodated by the surrounding matrix. Vagarali and Odette (1981) proposed a GB diffusion limited model in which void growth is constrained through inhibition of GB diffusion by GB carbides. The strain due to plating atoms on GBs was assumed to be accommodated by local plastic deformation in regions of inhibited GBs around carbides. Parthasarathy (1985) investigated the expansion rate of carbon and 21/4Cr–1Mo steels due to void growth during HTHA. It was assumed that the void growth is unconstrained, i.e. no opposing stress was considered to be imposed on the cavitated GBs from surrounding non-cavitated grains. The total expansion rate of the sample was assumed to be the sum of the expansion rate due to creep and due to the slowing of GB diffusion and surface diffusion processes. Similar to the previous work, it was assumed that each process is independent of the others.

Shewmon (1987) was the first to consider the effect of external stress and propose a model to account for the interaction between internal methane pressure and external stress. The void growth was calculated based on the coupling between the GB diffusion and creep of the surrounding matrix. It was assumed that the part of the boundary close to the void is expanding by GB diffusion and the rest by power-law creep. The model suggested that, under relevant HTHA conditions, the fracture is creep limited at all temperatures and stresses. Stone (1984) considered a constrained void growth model to study the kinetics of bubble growth in a 21/4Cr–1Mo steel under applied stress. He assumed that when void growth becomes constrained, the driving force for growing the void approaches zero, i.e. the magnitude of the developed back stress approaches that of the driving force for unconstrained void growth. As a result, the equivalent stress applied on the uncavitated grains is the sum of applied stress and the back stress. Using this equivalent stress, Stone calculated the creep rate of the uncavitated grains which he related to the expansion rate of the sample and the void growth. Chao (1987) developed a constrained cavity growth model in the absence of any external load to investigate HTHA of 21/4Cr–1Mo steel. A sphere with a cavitated facet inside another sphere was considered to represent cavitated and uncavitated grain boundaries, respectively. The inner sphere was assumed to have two rigid half spheres with voids between them that grow by GB diffusion (i.e. inserting atoms in between these two half spheres) such that a back stress develops. The back stress expanded the outer sphere by creep deformation and suppressed cavity growth in the inner sphere.

Needleman and Rice (1980) were the first to study the interaction of bulk creep deformation with GB dif-

fusion for creep cavitation applications. They obtained numerical solutions of void growth by creep and diffusion in a cylindrical unit cell subjected to uniaxial macroscopic tension. In the model, void growth was driven only by the remote stress, as there was not any internal pressure. Sham and Needleman (1983) extended the model of Needleman and Rice (1980) to multiaxial stress states to study void growth under higher triaxialities typical in crack growth situations. Van der Giessen et al. (1995) extended the results of Sham and Needleman (1983) for all stress triaxialities and presented an extension to their approximate closed-form expression to cover the entire stress triaxiality range and higher porosities (higher values of void radius to void spacing ratio), when interaction between voids becomes important.

Van der Burg et al. (1996) used the expressions proposed by Van der Giessen et al. (1995) to study unconstrained growth of voids under coupled creep and GB diffusion processes in 21/4Cr–1Mo steels. They assumed that the methane pressure inside the voids is always in equilibrium with the hydrogen gas pressure and carbon activity in the steel at a given temperature and computed the void growth for different carbides (M_3C, M_7C_3, and $M_{23}C_6$). The material was assumed to fail when the ratio of the void size $2a$ to the void spacing $2b$ reached $a/b = 0.7$. With this failure criterion, Nelson type curves for various applied loading conditions were obtained. The study showed that the applied external load can significantly influence the time to failure. The authors' calculations indicated that the creep contribution to cavity growth became significant only when the void grew to a sufficiently large fraction of void spacing b.

Van der Burg and Van der Giessen (1996a, b) investigated the effect of the surrounding grain interactions during void growth in a polycrystalline aggregate under HTHA conditions. They considered polycrystalline material with hexagonal grains under plane strain conditions and assumed that all GBs were covered with voids but with varying types and strengths of GB carbides that resulted in varying methane pressure distributions on each GB. It was assumed that void growth opens up the GBs by an amount proportional to the void volume. The authors' simulations showed that constrained deformation generates internal stresses that suppress void growth along boundaries with above-average methane pressure and increase void growth for other boundaries. It was noted that the lifetime does not simply scale with the amount of unstable carbides and that the presence of an external load reduced the time to failure. Van der Giessen and his co-workers (Van der Burg and Van der Giessen 1997; Schlogl and Van der Giessen 2001) proposed a continuum damage model for macroscopic assessment of components under HTHA conditions. They applied their model to a welded pressure vessel made of 21/4Cr–1Mo steel with different regions (i.e. weld metal, coarse-grained heat-affected zone, fine-grained heat-affected zone, and base metal) with corresponding different material properties and microstructures (such as creep properties and carbide compositions). The results showed that damage levels were different among the different regions and it was the different magnitude of methane pressure which developed in each region that was the main reason behind the variability of damage.

In a following study, Schlogl et al. (2000) derived the relations for the chemical potential of different elements in low alloy Cr–Mo steels (i.e. Fe, Cr, Mo, and V) with ferritic microstructures and calculated the equilibrium methane pressure associated with various types of carbides. Using the void growth expressions of Van der Giessen et al. (1995), they modeled the effect of decarburization on void growth through its effect on the creep resistance of the material (Schlogl et al. 2000). It was concluded that under practical HTHA conditions, decarburization has an insignificant effect on cavity growth. Schlogl et al. (2001) and Schlogl and Van der Giessen (2002) investigated the assumption that the pressure in the nucleated void quickly reaches equilibrium with the hydrogen gas environment and remains constant during void growth. They studied void growth in a unit cell by coupling the kinetics of carbide dissolution, diffusion of carbon and metal atoms from/to the carbides, diffusion of carbon atoms to void surfaces, and the kinetics of chemical reaction for methane generation. It was suggested that void growth and methane generation were coupled.

The preceding review of the literature shows that the early models managed to capture various qualitative aspects of HTHA as observed in experimental investigations. However, due to neglect of the interactions between the various processes underlying the damage development or the use of simple approximate approaches, those proposed models are not predictive. The most recent models on the other hand provide a more complete description of the various effects on the time to failure. However, due to their sophisticated and

very complex nature and the lack of experimental validation, they have not been adopted in the real word practice to advance the empirical models. This present work was initiated to review previous studies and assess how existing models could be improved. The objective is to stimulate interest and more work to improve the mechanistic models started in the 1980s. Better models should be applicable to all steels represented on the Nelson Curve diagrams, and should provide a more predictive fitness-for-service assessment of existing equipment and a better guidance for setting safe operating limits. HTHA models should also address the time to failure of components, and address parameters such as applied stress and material microstructure.

In this work, we present a model for grain boundary (GB) failure by HTHA based on the underlying deformation and fracture mechanisms. The model addresses growth of the pressurized voids along grain boundaries by accounting for their interaction with the creeping of the surrounding grains under constrained conditions. The objective is for the model to be simple to use while capturing the underlying chemo-mechanics. We revisited the constrained void-growth model of Stone (1984) and incorporated the interaction between void growth, creep of the surrounding matrix, and GB diffusion. Stone proposed a one-dimensional HTHA model in which void growth takes place only by diffusion of atoms along grain boundaries while the neighboring uncavitated grains geometrically constrain the growth—creep in the cavitated regions was neglected as being insignificant. In our model, we follow Stone's approach but incorporate the void growth model of Van der Giessen et al. (1995), in which coupled GB creep and GB diffusion processes are acting in concert. Lastly, as in previous models, we assumed pre-existing voids on the grain boundaries and therefore void nucleation is not accounted for in the present model.

2 High temperature hydrogen attack model

A schematic for the constrained void growth model is presented in Fig. 1. Regions A and B represent uncavitated and cavitated GBs, respectively. Force balance for the sections gives

$$\sigma_A(1 - f_b) + \sigma_B f_b = \sigma_\infty, \tag{1}$$

where f_b is the area fraction of the cavitated GBs, σ_A and σ_B are the stresses developed in regions A and B, respectively, and σ_∞ is the macroscopic stress applied remotely on both regions. Compatibility of deformation dictates that the total strain rate of cavitated and uncavitated regions be the same:

$$\dot{\varepsilon}_{\text{total}} = \dot{\varepsilon}_A^{\text{e}} + \dot{\varepsilon}_A^{\text{c}} = \dot{\varepsilon}_B^{\text{e}} + \dot{\varepsilon}_B^{cd}, \tag{2}$$

where superscripts e, c, and cd represent respectively deformation due to elasticity, creep, and creep combined with GB diffusion that results in void growth in the cavitated regions. The elastic deformation can be expressed in terms of the Young's modulus E as

$$\varepsilon_A^{\text{e}} = \frac{\sigma_A}{E},\ \varepsilon_B^{\text{e}} = \frac{\sigma_B}{E}. \tag{3}$$

For the creep deformation, we assume that the material obeys power law creep

$$\dot{\varepsilon}_A^{\text{c}} = \dot{\varepsilon}(\Theta)\left(\frac{\sigma_A}{\sigma_0}\right)^n, \tag{4}$$

where n is the creep exponent, σ_0 is a reference stress, $\dot{\varepsilon}(\Theta)$ is a reference strain-rate which depends on temperature Θ. For the strain rate $\dot{\varepsilon}_B^{cd}$ of the cavitated regions, we assume that it is associated with the volumetric growth of the cavities which is brought about by creep of the surrounding material as described by Eq. (4) and grain boundary diffusion. The corresponding volumetric growth rate is $\rho L^2 \dot{V}$, where the parameters L denotes the grain size, ρ the bubble number density on cavitated GBs, and $\dot{V}$ the rate of volume growth of an individual cavity. Next, assuming that the volume change of the cavities is accommodated by a fraction λ of the grain, i.e. λL^3, we calculate the strain rate $\dot{\varepsilon}_B^{cd}$ of the cavitated regions as

$$\dot{\varepsilon}_B^{cd} = \frac{\rho L^2 \dot{V}}{\lambda L^3} = \frac{\rho \dot{V}}{\lambda L}, \tag{5}$$

The volumetric growth rate $\dot{V}$, being brought about by coupled creep and GB diffusion processes, is calculated as in Van der Burg et al. (1996), which is elaborated next, and is a function of stress, σ_B, internal void pressure, p, and void geometry.

Van der Burg et al. (1996) considered voids along a GB with radius a, spacing between the voids $2b$, and tip angle of the spherical-caps shaped void ψ (see Fig. 2). The volume of the void is calculated as

$$V = \frac{4}{3}\pi a^3 h(\psi), \tag{6}$$

where $h(\psi) = [(1 + \cos\psi)^{-1} - \cos\psi/2]/\sin\psi$ is the void shape parameter. The voids were subjected to remote macroscopic axial and radial stress S and T,

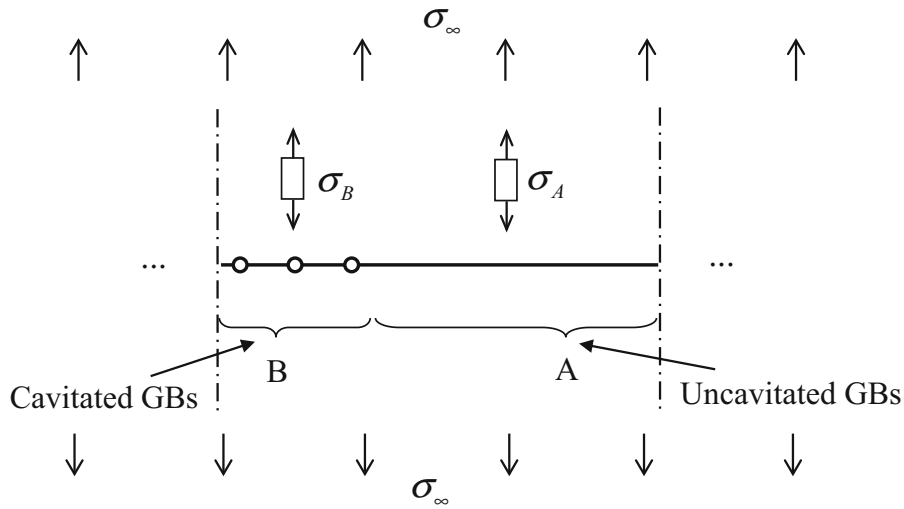

Fig. 1 Schematic of one-dimensional constrained cavity growth model for the study of HTHA kinetics. Void growth in the cavitated boundary will cause an increase in stress σ_A in the uncavitated grain region and decrease in stress σ_B in the cavitated region

respectively, and internal pressure p on the void surfaces. Extending the model of Van der Giessen et al. (1995) to account for the internal void pressure, Van der Burg et al. (1996) considered a simple superposition of a hydrostatic stress on the unit cell equal to the void pressure as shown in Fig. 3. Since creep is incompressible, the expressions of Van der Giessen et al. (1995) were adjusted by linking the internal pressure contribution to the applied external stresses. Thus, the void growth rate is calculated as equal to that of a void with no internal gas pressure and under remote macroscopic stresses

$$\begin{aligned} \sigma_{11}^{\infty} &= S + p, \\ \sigma_{22}^{\infty} &= \sigma_{33}^{\infty} = T + p, \\ \sigma_{12}^{\infty} &= \sigma_{13}^{\infty} = \sigma_{23}^{\infty} = 0. \end{aligned} \tag{7}$$

The remote mean stress $\sigma_{\mathrm{m}}^{\infty}$ and the effective stress $\sigma_{\mathrm{e}}^{\infty}$ associated with the stress state given in (7) are

$$\begin{aligned} \sigma_{\mathrm{m}}^{\infty} &= (S + 2T)/3 + p, \\ \sigma_{\mathrm{e}}^{\infty} &= \left|\sigma_{11}^{\infty} - \sigma_{22}^{\infty}\right| = |S - T|, \end{aligned} \tag{8}$$

where $|.|$ denotes absolute value. With the assumption that grains deform by power-law creep with creep exponent n, the effective creep strain rate due to the applied remote stresses can be described by

$$\dot{\varepsilon}_{\mathrm{e}} = \dot{\varepsilon}(\Theta) \left(\frac{\sigma_{\mathrm{e}}^{\infty}}{\sigma_0} \right)^n. \tag{9}$$

Van der Giessen et al. (1995) presented the rate of the volumetric growth of voids as

$$\dot{V} = \max \left[\left| \dot{V}_{\mathrm{cr}}^{\mathrm{L}} + \dot{V}_{\mathrm{diff}}^{\mathrm{L}} \right|, \left| \dot{V}_{\mathrm{cr}}^{\mathrm{H}} + \dot{V}_{\mathrm{diff}}^{\mathrm{H}} \right| \right], \tag{10}$$

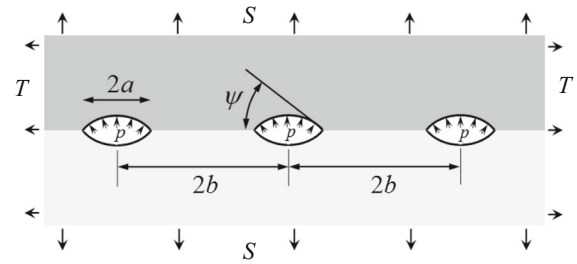

Fig. 2 Schematic of voids along a grain boundary facet under internal pressure p, macroscopic normal stress S and radial stress T (adapted from Van der Burg et al. 1996)

where the subscripts "cr" and "diff" denote void growth due to power-law creep and GB diffusion, respectively. The superscript L is for the case when the stress triaxiality $\sigma_{\mathrm{m}}^{\infty}/\sigma_{\mathrm{e}}^{\infty}$ is relatively low or when the porosity level a/b is relatively small and the superscript H is for high stress triaxiality or high porosity. The void volume growth rate due to creep is given by

$$\dot{V}_{\mathrm{cr}}^{\mathrm{L}} = \frac{3}{2} V \dot{\varepsilon}_{\mathrm{m}} \mathrm{sign}(\sigma_{\mathrm{m}}^{\infty}) \times \begin{cases} \left(\alpha_n + \beta_n \left| \frac{\sigma_{\mathrm{e}}^{\infty}}{\sigma_{\mathrm{m}}^{\infty}} \right| \right)^n, & \text{if } \left| \frac{\sigma_{\mathrm{m}}^{\infty}}{\sigma_{\mathrm{e}}^{\infty}} \right| \geq 1 \\ (\alpha_n + \beta_n)^n \left| \frac{\sigma_{\mathrm{e}}^{\infty}}{\sigma_{\mathrm{m}}^{\infty}} \right|^{n-1}, & \text{if } \left| \frac{\sigma_{\mathrm{m}}^{\infty}}{\sigma_{\mathrm{e}}^{\infty}} \right| < 1 \end{cases} \tag{11}$$

and

$$\dot{V}_{\mathrm{cr}}^{\mathrm{H}} = \frac{3}{2} V \dot{\varepsilon}_{\mathrm{m}} \mathrm{sign}(\sigma_{\mathrm{m}}^{\infty}) \left(\frac{1}{1 - (0.87a/b)^{3/n}} \right)^n \times \begin{cases} \left(\alpha_n + \frac{m}{n} \left| \frac{\sigma_{\mathrm{e}}^{\infty}}{\sigma_{\mathrm{m}}^{\infty}} \right| \right)^n, & \text{if } \left| \frac{\sigma_{\mathrm{m}}^{\infty}}{\sigma_{\mathrm{e}}^{\infty}} \right| \geq 1 \\ (\alpha_n + \frac{m}{n})^n \left| \frac{\sigma_{\mathrm{e}}^{\infty}}{\sigma_{\mathrm{m}}^{\infty}} \right|^{n-1}, & \text{if } \left| \frac{\sigma_{\mathrm{m}}^{\infty}}{\sigma_{\mathrm{e}}^{\infty}} \right| < 1 \end{cases} \tag{12}$$

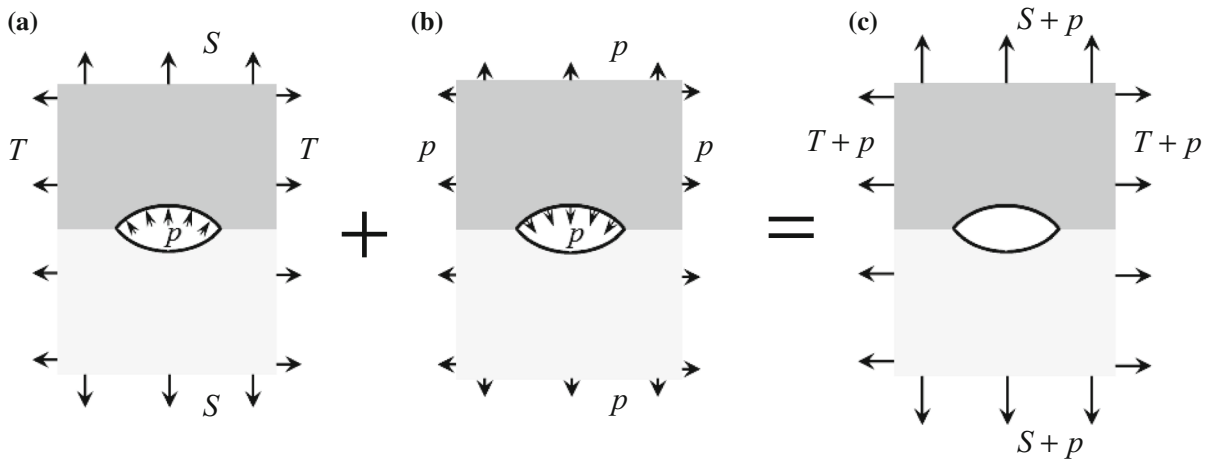

Fig. 3 Schematic of **a** the actual boundary stress for a unit cell with a void under HTHA conditions, **b** the superposed hydrostatic stress, and **c** the resulting stress state with stress-free cavity surface (adopted from Van der Burg et al. 1996)

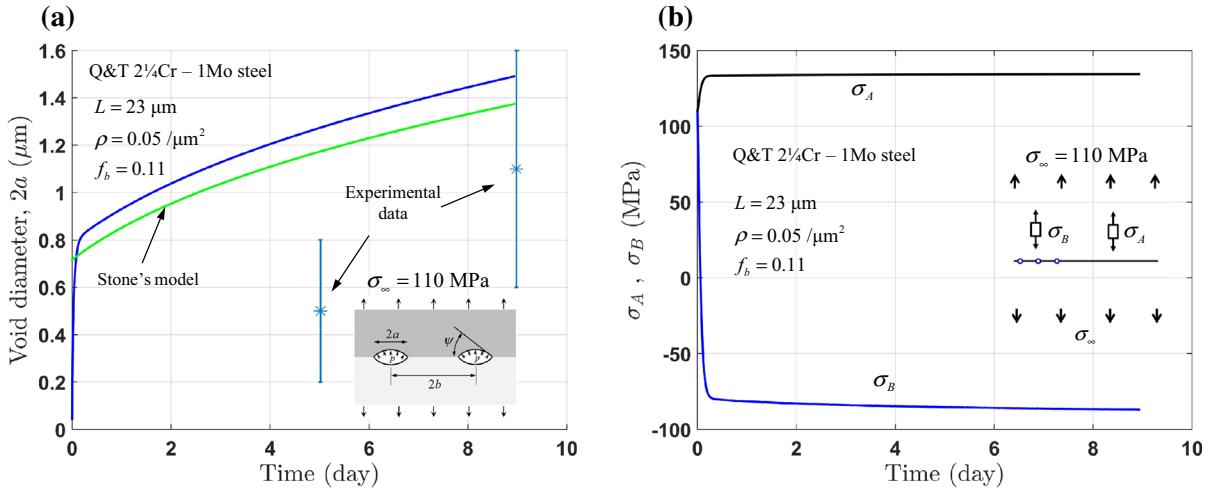

Fig. 4 Model predictions of constrained void growth for a 21/4Cr–1Mo steel in 13.8 MPa H_2 gas at 600 °C environment and under 110 MPa external stress σ_∞: **a** void diameter as a function of time and **b** stresses σ_B and σ_A on the cavitated and uncavitated regions, respectively. The steel is quenched and tempered with grain size $L = 23\,\mu$m and bubble number density on cavitated GBs $\rho = 0.05/\mu\text{m}^2$. The cavitated GB area fraction was assumed $f_b = 0.11$, the initial void diameter $2a_0 = 0.02b = 0.0447\,\mu$m with $2b$ being the bubble spacing, and the calculated bubble pressure was $p = 94.3$ MPa. The experimental data for the void growth and Stone's model predictions are also superposed (Stone 1984)

where $\dot{\varepsilon}_\text{m} = \dot{\varepsilon}(\Theta)\left|\sigma_\text{m}^\infty/\sigma_0\right|^n$, $\alpha_n = 3/(2n)$, $\beta_n = (n-1)(n+0.4319)/n^2$, and $m = \text{sign}(S-T)/\text{sign}(\sigma_\text{m}^\infty)$. The void growth rate due to diffusion is

$$\dot{V}_\text{diff}^\text{L} = \dot{V}_\text{diff}(f),\ \ f = \max\left[\left(\tfrac{a}{b}\right)^2, \left(\tfrac{a}{a+1.5L_{NR}}\right)^2\right]$$
$$\dot{V}_\text{diff}^\text{H} = \dot{V}_\text{diff}(f),\ \ f = \left(\tfrac{a}{b}\right)^2 \tag{13}$$

where $L_{NR} = (D(\Theta)\sigma_\text{e}^\infty/\dot{\varepsilon}_\text{e}^\infty)^{1/3}$ is the diffusion length parameter introduced by Needleman and Rice (1980) and

$$\dot{V}_\text{diff}(f) = 4\pi D(\Theta)\times\frac{S+p-\sigma_s}{\ln(1/f)-(3-f)(1-f)/2}, \tag{14}$$

in which $\sigma_s = (1-f)2\gamma_s \sin\psi/a$ is the sintering stress, $D(\Theta) = D_B\delta_B\Omega/k\Theta$ is the grain boundary diffusion

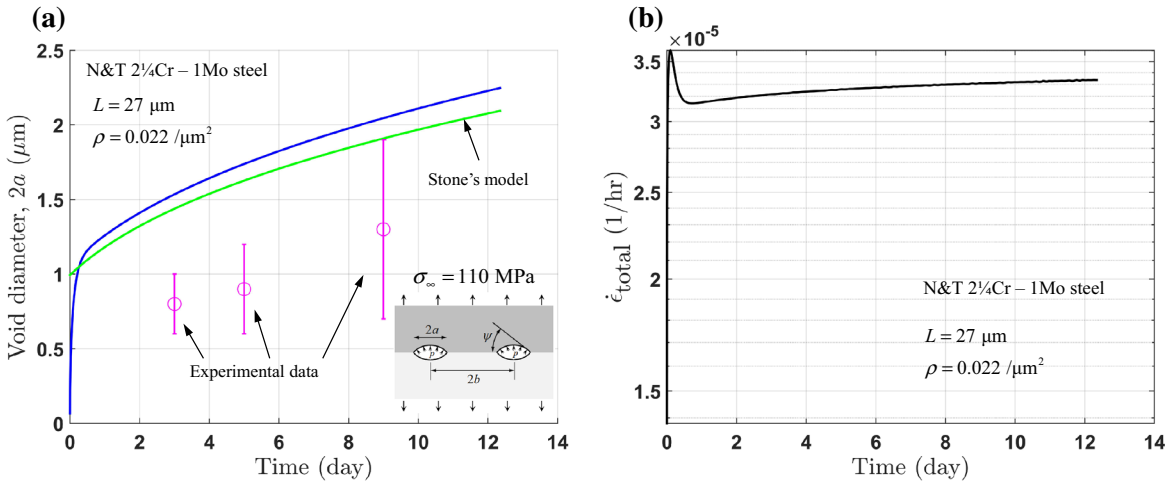

Fig. 5 Results of constrained void growth for the normalized and tempered 21/4Cr–1Mo steel in 13.8 MPa H_2 gas pressure at 600 °C under 110 MPa external stress: **a** void diameter as a function of time and **b** expansion rate $\dot{\varepsilon}_{\text{total}}$. The cavitated GB area fraction was taken $f_b = 0.11$, the initial void diameter $2a_0 = 0.02b = 0.0674\,\mu\text{m}$ with $2b = 1/\sqrt{\rho}$ being the bubble spacing, and the calculated bubble pressure was $p = 94.3$ MPa. The experimental data for the void growth and Stone's model predictions are also superposed (Stone 1984)

parameter, $D_B\delta_B$ is the boundary diffusion coefficient, Ω is the atomic volume, and k is Boltzmann's constant.

In order to determine the methane gas pressure inside the bubbles, we used the kinetic relation suggested by Grabke and Martin (1973) from their carburization and decarburization studies

$$\frac{dN_{\text{CH}_4}}{dt} = A\left(K_1\, C_C\, f_{\text{H}_2}^{3/2} - K_2\, f_{\text{CH}_4}/f_{\text{H}_2}^{1/2}\right), \quad (15)$$

where N_{CH_4} is the number of methane molecules, A is the reaction area, C_C is the carbon concentration at the surface in mol/m^3, f_{H_2} and f_{CH_4} are hydrogen and methane gas fugacities, K_1 and K_2 are respectively the rates for formation and decomposition of methane given by

$$\begin{aligned} K_1 &= 1.64\times10^{-3}\exp\left(-\frac{56{,}900}{R\Theta}\right)\ \frac{\text{m}}{\text{s MPa}^{3/2}} \\ K_2 &= 4.08\times10^{7}\exp\left(-\frac{213{,}400}{R\Theta}\right)\ \frac{\text{mol}}{\text{m}^2\text{s MPa}^{1/2}}, \end{aligned} \quad (16)$$

where $R = 8.314\,\text{J/mol K}$ is the universal gas constant. The fugacity of hydrogen f_{H_2} gas is assumed equal to the hydrogen gas pressure p_{H_2}, since the hydrogen pressure is generally much smaller than the methane gas pressure. We assumed chemical equilibrium between methane pressure inside the bubbles with hydrogen gas and carbides in steel and calculated the methane fugacity as

$$f_{\text{CH}_4} = f_{\text{H}_2}^2\, K_1\, C_C/K_2. \quad (17)$$

The non-equilibrium case is addressed in the discussion section. Having found the fugacity, we calculated the methane gas pressure p_{CH_4} through the relationship proposed by Odette and Vagarali (1982), i.e.

$$f_{\text{CH}_4} = p_{\text{CH}_4}\exp\left(C(\Theta)p_{\text{CH}_4}\right), \quad (18)$$

where

$$C(\Theta) = \begin{cases} 0.005\,\text{MPa}^{-1} \text{ for } f_{\text{CH}_4} < 10^3\,\text{MPa} \\ \frac{1.1875}{\Theta} + 3.0888\times10^{-3}\,\text{MPa}^{-1} \text{ for } 10^3\,\text{MPa} < f_{\text{CH}_4} < 10^4\,\text{MPa}, \\ \frac{2.375}{\Theta} + 1.1716\times10^{-3}\,\text{MPa}^{-1} \text{ for } f_{\text{CH}_4} > 10^4\,\text{MPa} \end{cases} \quad (19)$$

Finally the total gas pressure inside the bubble would be the summation of the methane and hydrogen gas pressures, $p = p_{\text{H}_2} + p_{\text{CH}_4}$.

3 Numerical simulation results in the presence of external stress

We simulated void growth in 21/4Cr–1Mo steel for which experimental data for HTHA is available. Stone (1984) performed HTHA experiments on two heats of 21/4Cr–1Mo steel, quenched and tempered (Q&T) and

normalized and tempered (N&T), and measured the void growth due to combined external load and internal bubble pressure. We assumed that the elastic modulus of the 21/4Cr–1Mo steel varies with absolute temperature as Θ (Davis 1997)

$$E(\Theta) = 241.25 - 0.09063 \times \Theta \text{ GPa}. \tag{20}$$

For the creep parameters in Eq. (4), experiments by Klueh (1980) give

$$\dot{\varepsilon}(\Theta) = \dot{\varepsilon}_0 \exp\left(-\frac{Q_v}{R\Theta}\right),\ n = 6.75,\ \sigma_0 = 1 \text{ MPa},\\ Q_v = 320 \text{ kJ/mol},\ \dot{\varepsilon}_0 = 5.69 \times 10^{-4}/\text{s}. \tag{21}$$

The boundary diffusion is $D_B\delta_B = 1.1 \times 10^{-12} \exp(-174,000/R\Theta)$ m^3/s, the atomic volume $\Omega = 1.18 \times 10^{-29}$ m^3 (Frost and Ashby 1982), $\psi = 78.5°$, and the surface free energy $\gamma_s = 1.95$ J/m^2 (Chuang et al. 1979). The distance between bubbles on the cavitated grain boundaries is calculated as $2b = 1/\sqrt{\rho}$, where the experimental observations for the bubble density ρ are used for each case, and the initial void radius a_0 is such that $a_0/b = 0.01$. It should be noted that the assumption of a small value for a_0 does not significantly affect the void growth results (Shih and Johnson 1982; Van der Burg et al. 1996) if the combined effect of applied stress S and internal void pressure p overcomes the sintering stress σ_s (see Eq. 14). This is related to the fact that, as a void starts to grow, the sintering stress decreases rapidly ($\sigma_s \propto 1/a$). For the fraction of the grain τ that accommodates the void growth, we assumed a value of 1/3 in Eq. (5). The effect of this assumption on void growth predicted by the present model and the model of Stone is further investigated in "Appendix B". To calculate the methane pressure, the concentration of carbon on the bubble surface in C_C Eq. (17) is given by

$$C_C = 6577.85 \times a_C \times C_{\text{gr}},\\ C_{\text{gr}} = 66.79 \exp\left(-\frac{68,700}{R\Theta}\right), \tag{22}$$

where C_{gr} is the graphite solubility in ferrite in wt. % (Darken and Gurry 1953), a_C the carbon activity in 21/4Cr–1Mo steel, and the mass density of steel in the calculation of the coefficient for the unit conversion from wt.% to mol/m^3 is 7900 kg/m^3 (Darken and Gurry 1953). For the 21/4Cr–1Mo steel, the carbon activity is reported between 0.1 and 0.3 (Chao 1987), and in our calculations we considered $a_C = 0.2$ for simplicity.

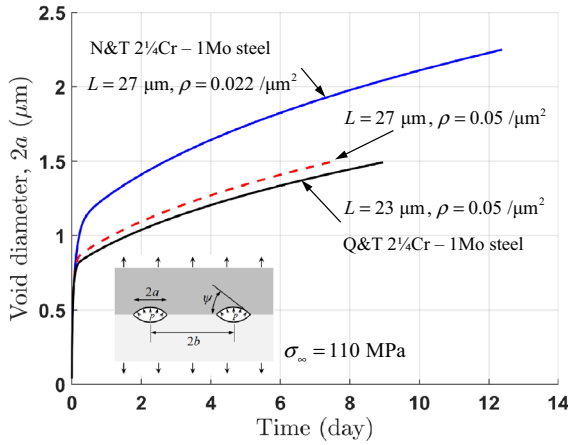

Fig. 6 Effect of the grain size L and bubble number density ρ on model predictions in 13.8 MPa H_2 gas pressure at 600 °C under 110 MPa external stress For all cases, the void diameter at failure over the void spacing ratio was assumed $(a/b)_{cr} = 1/3$, the cavitated GB area fraction $f_b = 0.11$, and the initial void diameters $2a_0 = 0.02b = 0.0447$ and 0.0674 μm respectively for $\rho = 0.05$ and 0.022/μm^2. The calculated pressure in the bubble was $p = 94.3$ MPa

Equations (1) through (5) were integrated for the Q&T 21/4Cr–1Mo steel in a hydrogen gas pressure of 13.8 MPa, temperature of 600 °C, and with an externally applied stress of 110 MPa. The Q&T steel had a grain size $L = 23$ μm and a bubble number density per cavitated grain $\rho = 0.05/\mu\text{m}^2$. The equilibrium gas pressure inside the bubbles is $p = p_{H_2} + p_{CH_4} = 94.3$ MPa. The evolution of the void diameter is shown in Fig. 4. Initially the void grows rapidly until the deformation constraint sets in which causes the growth to slow down as dictated by the creep deformation of the uncavitated grains (Fig. 4a). The experimentally determined void diameter after a given exposure time is also depicted in Fig. 4a. One may claim that the model prediction for the rate of void growth is in reasonable agreement with that of the experimental data. The void growth results from Stone's model[1] are also superposed on Fig. 4a. It is interesting that Stone's predictions are similar to the present model's predictions, and this is despite the fact that creep in the cav-

[1] See "Appendix A" for the details of Stone's model. In order to calculate the stress on the uncavitated GBs, Stone (1984) assumed that the void growth rate approaches zero. There was a minor mistake in the calculation of Stone and the correct form for the uncavitated GB stress is $\sigma_A \approx (1/(1-f_b))\,\sigma_\infty + (f_b/(1-f_b))\,p$. This equation was used to plot the void growth predictions in the figures for Stone's model.

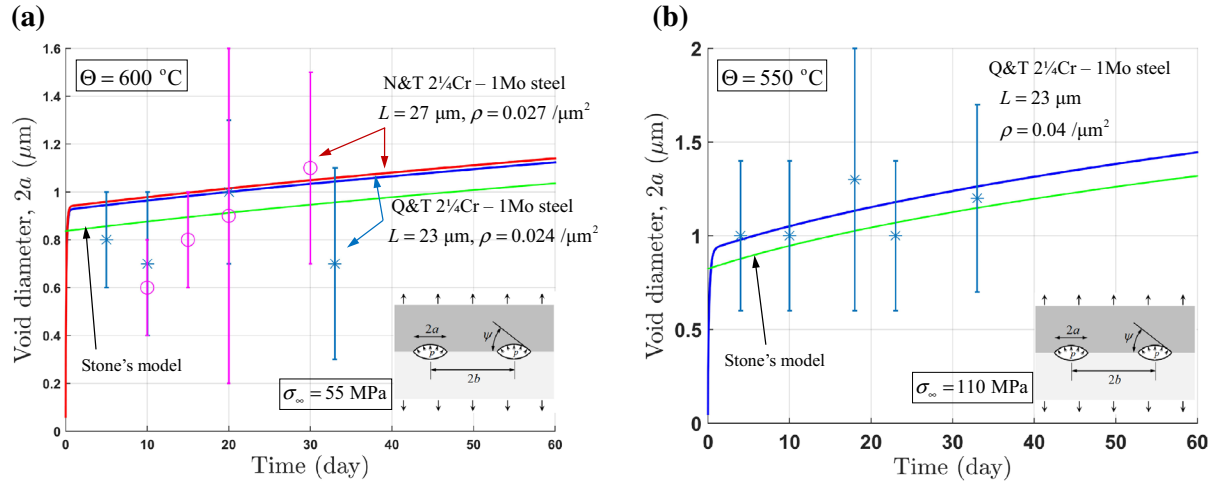

Fig. 7 Void growth results for cavitated GB area fraction $f_b = 0.11$: **a** quenched and tempered and normalized and tempered 21/4Cr–1Mo steel in 13.8 MPa H_2 gas pressure at 600 °C under 55 MPa external stress. The calculated bubble pressure was $p = 94.3$ MPa and the initial void diameters $2a_0 = 0.02b = 0.0645$ and 0.0609 μm respectively for $\rho = 0.024$ and $0.027/\mu m^2$, where $2b = 1/\sqrt{\rho}$ is the bubble spacing **b** quenched and tempered steel in 13.8 MPa H_2 gas pressure at 550 °C under 110 MPa external stress. The calculated bubble pressure was $p = 144.4$ MPa and the initial void diameter 0.050 μm. The experimentally determined void diameters (data points with error bars) and the Stone's model predictions for each case are also shown (Stone 1984)

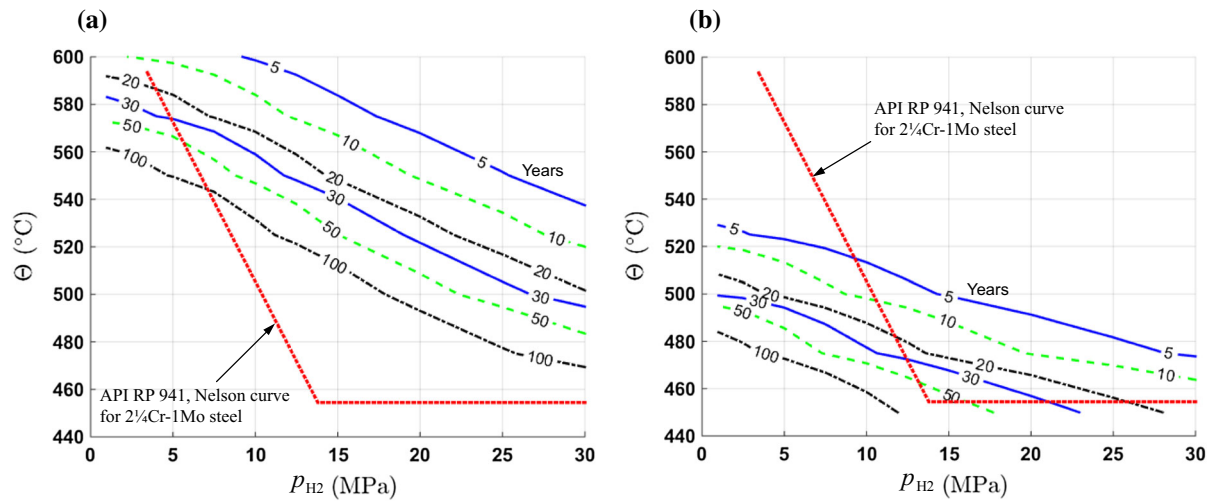

Fig. 8 Contour plots of time to failure in years plotted on a Nelson type graph for the quenched and tempered 21/4Cr–1Mo steel under applied stress **a** $\sigma_\infty = 50$ MPa and **b** $\sigma_\infty = 100$ MPa, and: bubble pressure $p = p_{H_2} + p_{CH_4}$ with p_{CH_4} calculated from Eqs. (16)–(18), grain size $L = 23$ μm, void density $\rho = 0.05/\mu m^2$, initial void diameter $2a_0 = 0.02b = 0.0447$ μm, cavitated GB area fraction $f_b = 0.11$, and critical void size to void spacing ratio for failure $(a/b)_{cr} = 1/3$. The Nelson curve for 21/4Cr–1Mo steel from API RP 941 (2016) is also superposed on the figures

itated grains is neglected in Stone's model. This is explained by the fact that the void growth in Fig. 4 is controlled by GB diffusion because the Needleman and Rice nondimensionalized diffusion length $L_{NR}/a_0 = (D(\Theta)\sigma_\infty/\dot{\varepsilon}_\infty)^{1/3} = 552.3$ is larger than 20 (Needleman and Rice 1980). For the calculation of

L_{NR} we considered $\sigma_\infty = 110$MPa and $\dot{\varepsilon}_\infty = A\sigma_\infty^n$, where $A = 4.0589 \times 10^{-23}$ $(\text{MPa})^{-n}/\text{s}$ and $n = 6.75$ are creep parameters given in (21). However, Stone's model is not expected to do well when void growth is controlled by creep or the interaction between creep and GB diffusion. For the void growth in Q&T steel, L_{NR}/a decreases from 552.3 upon growth initiation to 16.6 at failure. Hence, close to failure, void growth takes place by both GB diffusion and creep as the nondimensional diffusion length is close to 20. For a larger applied stress such as $\sigma_\infty = 200$ MPa, L_{NR}/a changes from 175.6 to 5.3, a case in which creep straining become significantly close to failure. Figure 4b shows the variation with time of the stresses in the cavitated and uncavitated regions. We assumed that the stresses in both regions were initially $\sigma_A = \sigma_B = \sigma_\infty = 110$ MPa. The area fraction of the cavitated GBs was taken $f_b = 0.11$, which represents cavitation of approximately one out of every 3 GBs. Stone's experiments (Stone 1984) showed that the Q&T 21/4Cr–1Mo steel in 13.8 MPa H_2 gas at 600 °C environment under 110 MPa external load failed after 9 days. In our simulations, we chose the critical value for the void diameter to be $(a/b)_{cr} = 1/3$ so that the time to failure in the simulation matches that in the experiments.

Under the same environmental conditions (i.e. 13.8 MPa H_2 gas pressure at 600 °C) and external load ($\sigma_\infty = 110$ MPa), we also simulated void growth in the N&T 21/4Cr–1Mo steel. The N&T steel had a grain size $L = 27\,\mu$m, which was slightly larger than that for the Q&T steel, but the bubble number density determined for the N&T steel was much smaller, $\rho = 0.022/\mu\text{m}^2$. Except for the grain size and the bubble density, we assumed the other parameters, i.e. the material properties the void geometry and spacing and the carbon activity, for the N&T steel to be the same as those for the Q&T steel. In general, the simulation results for the N&T steel also show a trend for the void growth rate similar to that of the experimental data (Fig. 5a), with the corresponding nondimensionalized length being initially $L_{NR}/a_0 = 366.3$ and reducing to $L_{NR}/a = 16.6$ at failure. The expansion rate of the specimen is plotted in Fig. 5b. At the beginning, the expansion rate increases rapidly up to a maximum which is attained upon the setting in of the constraint, and thereafter it drops and finally reaches a steady state value. This decrease of the expansion rate is not significant because the value of 110 MPa externally applied stress on the sample is rather high. In the case of lower external stress, the decrease can be several orders of magnitude as will be discussed in the discussion section.

The model predictions for the void diameter in the Q&T (Fig. 4a) and N&T (Fig. 5a) 21/4Cr–1Mo steel are compared in Fig. 6. As can be seen, the difference in the grain size does not have a significant effect on the void growth, but the reduction of the void bubble density from 0.05 to $0.022/\mu\text{m}^2$ causes the magnitude of the void diameter at which the constraint effect sets in to increase, which in turn results in larger void growth.

Void growth predictions under a smaller external load, $\sigma_\infty = 55$ MPa, for both heats of the same steel in 13.8 MPa H_2 gas pressure and 600 °C are compared in Fig. 7a with corresponding experimental measurements and the predictions of the Stone model. Reduction of the external load by a factor of 2 decreases the void growth rate markedly. Results for void growth in Q&T 21/4Cr–1Mo steel at a lower temperature, $\Theta = 550\,°\text{C}$, in 13.8 MPa H_2 gas pressure under $\sigma_\infty = 110$ MPa are presented in Fig. 7b and compared with the Stone's experimental data and model. The equilibrium gas pressure inside the bubbles at $\Theta = 550\,°\text{C}$ is $p = p_{H_2} + p_{CH_4} = 144.4$ MPa. As expected, Fig. 7 shows that reducing the applied stress or the temperature results in decreased growth rates as both stress and temperature reductions decrease the creep rate. It also shows that the results are in good agreement with the experimental data.

For the Q&T 21/4Cr–1Mo steel with grain size $L = 23\,\mu$m, we calculated the time to failure as a function of hydrogen gas pressure and temperature. We assumed failure to take place when the void grows to a critical size, $(a/b)_{cr} = 1/3$. Although the bubble density changes with temperature, pressure, and stress, we assumed a fixed density, $\rho = 0.05/\mu\text{m}^2$, which is the most severe case resulting in a conservative calculation of the failure time. The results under external stress $\sigma_\infty = 50$ and 100 MPa are plotted in Fig. 8a, b, respectively. Superposed on the figures is the Nelson curve suggested for 21/4Cr–1Mo steel by the American Petroleum Institute (API RP 941 2016). The operation under a given temperature and hydrogen pressure is deemed safe under the Nelson curve. Under $\sigma_\infty = 50$ MPa, steels operating in hydrogen gas pressure and temperature conditions below much of the API Nelson curve will be safe for over 100 years according to our calculations. However, for applied stress equal to 100 MPa, the calculations show that the steel is suscep-

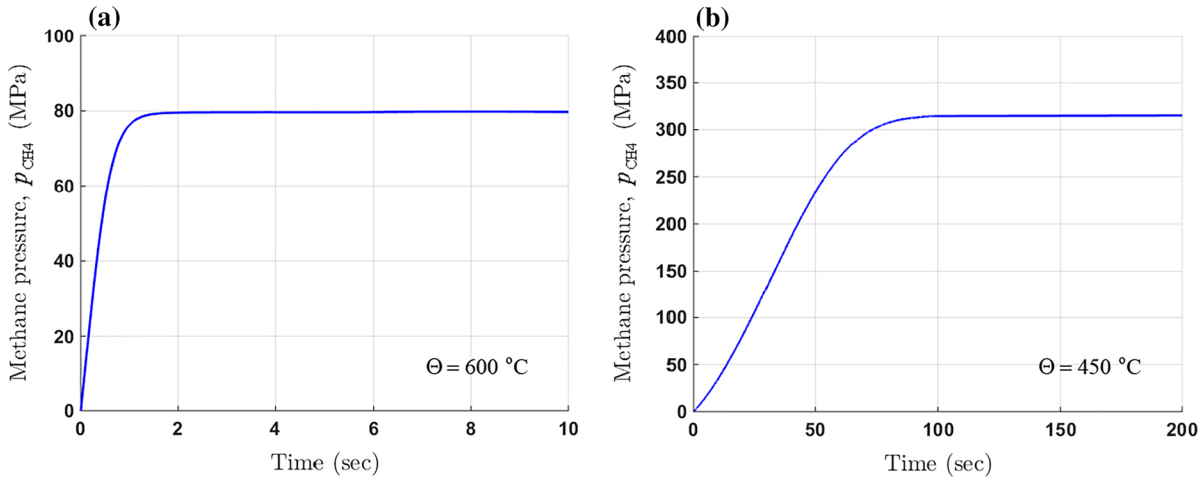

Fig. 9 Evolution of methane pressure p_{CH_4} inside a bubble in 21/4Cr–1Mo steel in 13.8 MPa H_2 gas pressure at **a** 600 °C and **b** 450 °C

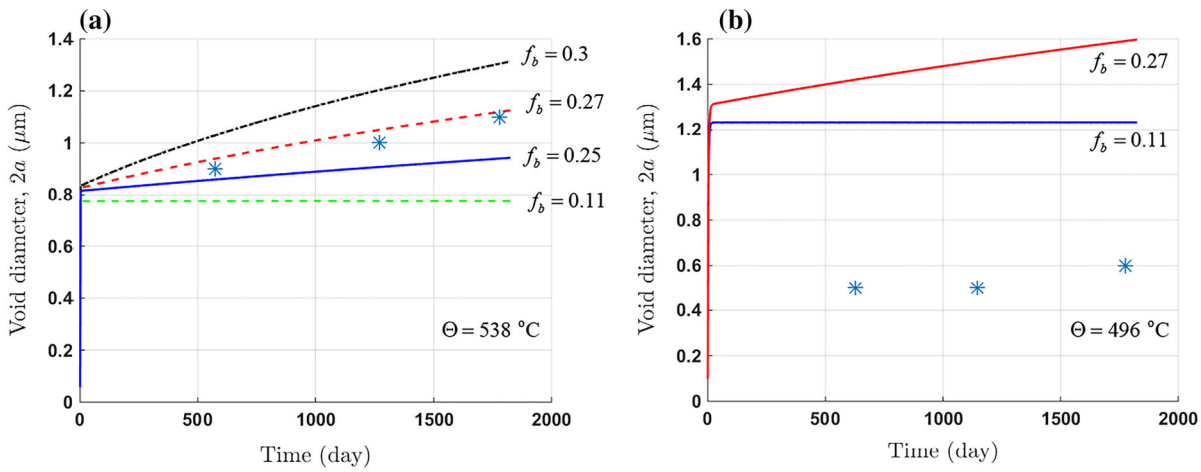

Fig. 10 Void growth results under no external stress for quenched and tempered 21/4Cr–1Mo steel with grain size $L = 10\,\mu$m and various area fractions of the cavitated GBs, f_b, in 20.7 MPa H_2 gas pressure at: **a** 538 °C and **b** 496 °C. The data points show the experimental measurements of Erwin (1982). At 538 °C and 496 °C the bubble densities were assumed $\rho = 0.03/\mu\text{m}^2$ and $\rho = 0.01/\mu\text{m}^2$ in accordance with the experimental observations, the initial void diameters were $2a_0 = 0.02b = 0.0577$ and 0.1 μm with $2b = 1/\sqrt{\rho}$ being the bubble spacing, and the bubble pressures were calculated as $p = 244.2$ and 339.0 MPa, respectively

tible to failure much earlier, with the failure conditions becoming more severe at higher temperatures.

It should be noted that we have used simple assumptions to obtain the void growth and failure time over a wide range of hydrogen gas pressures and temperatures. For example, a constant carbon activity was assumed for the steels, although the activity will vary from heat to heat and between the base and weld metals, a factor which is not addressed in this study. Moreover, the calculated curves are valid to the extent that the various underlying deformation and failure mechanisms are correctly described. Therefore, the presented failure time curves should not be considered as final definitive results or substitutes for the Nelson curves. Rather, they should be viewed as a first step toward replacing the phenomenological curves by curves that are obtained through mechanistic understanding.

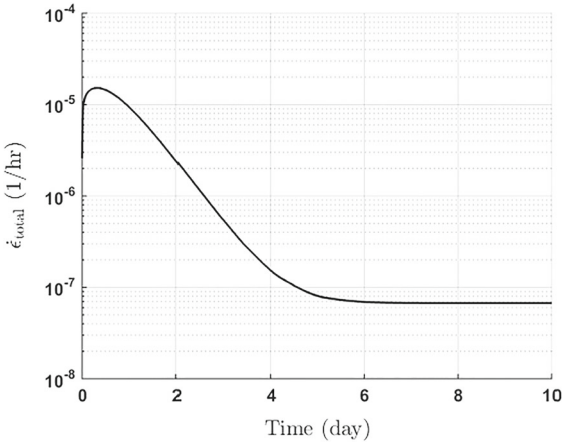

Fig. 11 Calculated expansion rate $\dot{\varepsilon}_{\text{total}}$ for quenched and tempered 21/4Cr–1Mo steel under no external stress after exposing the specimen to 20.3 MPa H_2 gas pressure at 550 °C. The grain size was $L = 50\,\mu\text{m}$ and the cavitated GB area fraction $f_b = 0.27$

Another assumption in our calculation of void growth was the equilibrium between the methane gas pressure with hydrogen gas and carbides; an assumption which an investigation into the kinetics of the reaction shows is valid. In order to investigate the effect of methane generation kinetics, we solved Eq. (15) coupled with the void growth Eqs. (1) through (5). Integration of Eq. (15) provides the number of methane molecules in the bubble, which is related to methane pressure through $p_{CH_4} = Z N_{CH_4} R\Theta / V$, where Z is the compressibility coefficient (see Odette and Vagarali 1982) and V is the bubble volume as given by Eq. (6). The results show that accounting for the methane generation kinetics has an insignificant effect on the void growth evolution. As shown in Fig. 9a, under 13.8 MPa H_2 gas pressure at 600 °C and no external stress, methane pressure reaches equilibrium within seconds. At 450 °C, the time for methane pressure to reach equilibrium is prolonged to a couple of minutes (Fig. 9b) but it is still negligible in comparison with the life of the steel, which can be on the order of years or even decades. Therefore, we conclude that the methane generation kinetics does not seem to play a significant role in void growth.

4 Discussion

Numerical simulations were presented for void growth in 21/4Cr–1Mo steels under HTHA conditions with an externally applied stress. The results show that voids on the cavitated GBs experience rapid initial growth until they become constrained by the uncavitated regions, with their growth rate thereafter being controlled by the creeping rate of the uncavitated sections. In this section, we will discuss the application of our model to void growth for HTHA under no external stress.

Erwin (1982) studied bubble size and density in the Q&T 21/4Cr–1Mo steels in 20.7 MPa (3000 psi) hydrogen gas at 496 °C (925 °F) and 538 °C (1000 °F) for various exposure times. The average grain size was $L = 10\,\mu\text{m}$ and the bubble number densities on cavitated grains were about $\rho = 0.03/\mu\text{m}^2$ and $\rho = 0.01/\mu\text{m}^2$, at 498 and 538 °C, respectively. Figure 10 shows our model's predictions for the void size evolution simulating Erwin's experimental conditions. The bubble pressures at 496 °C and 538 °C in hydrogen gas pressure 20.7 MPa are $p = 244.2$ and 339.0 MPa, respectively. The results show that with the area fraction of the cavitated GBs $f_b = 0.11$, that we assumed when we compared our model's predictions with the experimental data under external stress, the model displays insignificant void growth during 5 years of exposure after initial growth. On the other hand, a parametric study we performed over the cavitated GB area fraction f_b at $\Theta = 538$ °C (Fig. 10a) shows that with $f_b = 0.27$ the model predictions reproduce the experimental data for the void size evolution. At $\Theta = 496$ °C (Fig. 10b), the model furnishes much larger void growth in comparison to the experimental data. It is known that at lower temperatures, processes such as carbon dissolution or diffusion that assist void growth become slower. It has been reported that the expansion rate for some 21/4Cr–1Mo steels at 500 °C dropped to negligible levels after several hours (Yu and Shewmon 1981; Shewmon and Yu 1982; Parthasarathy et al. 1985). This disagreement between our model predictions and the experimental void expansion rates at low temperatures is an indication that our HTHA model needs to be improved in order to also address the reaction(s) that control void growth at lower temperatures (Schlogl et al. 2001).

Shewmon and co-workers (Yu and Shewmon 1981; Shewmon and Yu 1982; Parthasarathy et al. 1985) measured the expansion rate for different heats of 21/4Cr–1Mo steels under HTHA. Several sequences of change in hydrogen gas pressure and temperature were used to obtain the expansion rate at various conditions. After each change in hydrogen gas pressure or temperature,

Table 1 Comparison of the model predictions for the steady-state expansion rate, $\dot{\varepsilon}_{\text{total}}$, with experimental results for quenched and tempered 21/4Cr–1Mo steel at various temperatures, Θ, and hydrogen gas pressures, p_{H_2}. The experimental data were taken from different sets of experiments performed on the base metal with average grain size of about $L = 50\,\mu\text{m}$ (Parthasarathy et al. 1985). For the numerical calculations, it was assumed that $L = 50\,\mu\text{m}$ and the cavitated GB area fraction $f_b = 0.27$

Θ (°C)	p_{H_2} (MPa)	Experimental results	Numerical calculations	
		Expansion rate (10^{-8}/h)	Bubble pressure p (MPa)	$\dot{\varepsilon}_{\text{total}}$ (10^{-8}/h)
500	20.3	< 1, 1.3, 1.4, 1.9	324.9	5.5
520	20.3	2.5	271.6	4.9
550	20.3	3.8, 6.9, 10.9, 11.4	220.2	6.7
565	20.3	10.2, 20.8	197.9	7.4
580	20.3	19.4, 19.8, 22.4	177.8	7.8
590	20.3	37.8	165.4	7.9
580	20.3	22.6, 29	177.8	7.8
580	16.9	10, 12.9	143.9	1.7
580	13.5	3.6, 7.9	108.6	0.22
550	13.5	3.3, 3.4	140.7	0.28
550	16.9	4.2	181.9	1.8
550	20.3	6.2	220.2	6.7

these researchers observed a transient in expansion rate before reaching a steady-state. For example, after changing the temperature from 500 to 550 °C while the hydrogen pressure was 20.3 MPa, steady-state expansion rate was reached after about 50 h (Parthasarathy et al. 1985). The steady-state expansion rate depended on hydrogen gas pressure and temperature while the sequence history did not significantly affect its value. Using Eq. (2), we calculated the expansion rate for the Q&T 21/4Cr–1Mo steel with grain size $L = 50\,\mu\text{m}$ and cavitated GB area fraction $f_b = 0.27$ in 20.3 MPa hydrogen gas and 550 °C. The numerical results plotted in Fig. 11 exhibit the same behavior as observed in the experiment but with a longer transient time. Table 1 shows the calculated gas pressure inside the bubble, p, and the steady-state expansion rates, $\dot{\varepsilon}_{\text{total}}$, corresponding to various sequences of hydrogen gas pressure and temperature changes as reported by Parthasarathy et al. (1985). The expansion rate trends in the numerical calculations were similar to those in the experiments as the temperature Θ and hydrogen gas pressure p_{H_2} were changed, though, the magnitudes were different. As the temperature was raised from 500 to 590 °C the expansion rate in the experiments in 20.3 MPa hydrogen gas increased by a factor of 20 whereas the numerical calculations show an increase by less than a factor of 2. On the other hand, increasing the hydrogen gas pressure from 13.5 to 20.3 MPa at 550 °C increased the expansion rate by about a factor of 2 in the results of the Parthasarathy et al. (1985) whereas the calculations showed an increase by about a factor of 20. These comparisons indicate that our model underpredicts the temperature effect and overpredicts the hydrogen gas pressure effect on the void expansion rate. These discrepancies may be due to inaccuracies in the creep model (cf. Eq. 4) underlying the present numerical calculations. The model of Eq. (4) neglects the hydrogen effect on creep. In addition, the discrepancies may be due to inaccuracies involved in the calculation of the methane equilibrium pressure or the neglect of void nucleation.

5 Concluding remarks

We have presented a simple constraint-based void growth model for HTHA of carbon steels combining the most useful aspects of previous models to capture the salient physical processes involved in the phenomenon. The constraint arises from the fact that some GBs are cavitated while others are not and the uncavitated ones exert an opposing stress to void growth on cavitated grains. The model rather accurately accounts

for the interaction between creep and grain boundary diffusion for void growth. When the model is complemented with a failure criterion, i.e. a critical ratio of void size to inter-void spacing, it can be used for lifetime predictions. In the case of void growth in 21/4Cr–1Mo steel exposed to high temperatures and high hydrogen gas pressures under uniaxial loading, the model predictions were in good correlation with experimental data sets for void growth. We also investigated the effect of the methane generation kinetics on void growth. For the temperature ranges of interest for 21/4Cr–1Mo steel, the results show that the kinetics of methane generation based on the Grabke and Martin (1973) equations is not rate-limiting, so accounting for it in the model does not appear to significantly influence the model predictions.

A key parameter of the model is the area fraction of the cavitated GBs f_b. Under external stress, the model predictions are in good agreement with the experimental results when $f_b = 0.11$. However, in the absence of stress, $f_b = 0.27$ is needed in order to get a good fit with the experimental results of void growth for a quenched and tempered 21/4Cr–1Mo steel at 538 °C and hydrogen gas pressure of 20.7 MPa. For void growth at 496 °C and 20.7 MPa hydrogen gas under no external stress, experiments showed very small growth which remained almost constant over several years. However, the model overpredicted those experimental results, a fact we attributed to rate-limiting processes at low temperatures not accounted for in the model. For example, the kinetics of carbon dissolution can impact the methane generation as discussed by Schlogl et al. (2001). Perhaps combining the present model with the rate of carbide dissolution for the determination of the methane pressure (Schlogl et al. 2001) can improve the predictive capabilities of the model at lower temperatures. Lastly, comparison of the model expansion rates with experimentally obtained rates in the absence of external stress showed similar trends in the change of the expansion rate as hydrogen gas pressure and temperature were varied. More specifically, for the 21/4Cr–1Mo steel, the model underpredicted the change of the expansion rate as a function of temperature and overpredicted the corresponding rate as a function of hydrogen gas pressure.

The model lifetime predictions under uniaxial loading were discussed relative to the Nelson curve for the 21/4Cr–1Mo steel in the temperature vs. hydrogen pressure diagram for two specific cases of the applied stress, 50 and 100 MPa. Although the model is simple and "one-dimensional," it is mechanistic and capable of delineating the safe/no-safe regimes in the diagram as shown in Fig. 8.

The deviation of the model's Nelson-type curve predictions from the API Nelson curve for the 21/4Cr–1Mo steel can be attributed to various factors. For example, we assumed that over a wide range of hydrogen pressures and temperatures, the creep mechanism, the failure criteria, and the material properties at failure remain the same. Different creep mechanisms can be dominant from one temperature range to another and this will influence the model predictions. In fact, the experimental data (Klueh 1980) show that the creep exponent for 21/4Cr–1Mo steel at 454 °C is different from that at 510 and 566 °C, which is an indication of creep mechanism change between 454 and 510 °C. Similarly, temperature can influence significantly the material resistance to failure and hence, the failure condition for the 21/4Cr–1Mo steel above 550 °C may be different from that below 500 °C. We assumed that failure took place when the size of a growing void reached 1/3 of the spacing between the voids. This assumption can be simplistic, as the temperature and methane gas pressure inside the voids can influence the failure process. Moreover, the presence of hydrogen can further complicate the problem as hydrogen is known to accelerate the creep rate. Therefore, the failure curves we calculated should be viewed as a first step toward the development of a methodology to establish Nelson curves that are mechanistic and not phenomenological.

In summary, the present model yielded satisfactory predictions for void growth in HTHA under externally applied load but it needs to be improved for the case of no external load. It seems that under the conditions examined in this paper the degradation of the material under external load is dominated by the externally applied stresses whereas the internal gas pressure has a smaller effect. The relationship between the methane pressure and the hydrogen gas pressure at a given temperature was calculated using a relationship derived for a free surface at very high temperatures; the kinetics may be different on the surface of the pressurized bubble, and this difference could profoundly affect the results in the absence of external load. Lastly, void nucleation may be different in the presence or absence of the external load. The advantage of the present model is the ability to make adjustments to account for these

physical aspects of the process, which will be the focus of future work.

Acknowledgements The authors would like to acknowledge the funding and technical support from BP through the BP International Centre for Advanced Materials (BP-ICAM) which made this research possible.

Appendix A: Stone's model (Stone 1984)

Stone proposed a constrained void growth model for bubble growth under applied stress (Stone 1984). He considered that when void growth becomes constrained the driving force that grows the void approaches zero. Neglecting elasticity and the effect of creep, Stone calculated the void growth after it becomes constrained as

$$a_S = a_S^0 \left(1 + K_S t\right)^{1/3}, \tag{23}$$

where

$$a_S^0 = \left(\frac{3\lambda L(\sigma_\infty + p)}{4\pi\rho E}\right)^{1/3}, \quad K_S = \frac{E\dot{\varepsilon}_A^{\mathrm{c}}}{\sigma_\infty + p} \tag{24}$$

a_S^0 is the radius at which the constraint sets in, t is time, λ is the fraction of the grain that accommodates the void growth, L the grain size, σ_∞ the macroscopically applied stress, p the internal void pressure, ρ the bubble number density on cavitated GBs, E the Young's modulus of elasticity, and $\dot{\varepsilon}_A^{\mathrm{c}}$ the creep rate in uncavitated grain boundaries. There was a minor mistake in the calculation of the uncavitated GB stress σ_A and the correct form is

$$\sigma_A = \frac{1}{1 - f_b}\sigma_\infty + \frac{f_b}{1 - f_b}p. \tag{25}$$

This equation was used to plot the void growth results shown in Figs. 4, 5, and 7 for Stone's model. Stone considered in Eq. (5) that $\lambda = f_b$ for the fraction of the grain which though seems to be rather small as we elaborate next in "Appendix B".

Appendix B: Effect of parameters λ and f_b on void growth

In order to investigate the effect of the fraction of the grain that accommodates the void growth, λ, and the area fraction of the cavitated grains, f_b, on the constrained void growth results, we simulated void growth for Q&T and N&T 21/4Cr–1Mo steels with a hydrogen gas pressure of 13.8 MPa, temperature 600 °C, and $\sigma_\infty = 110$ MPa for various values of λ and f_b. As mentioned in "Appendix A", Stone (1984) assumed

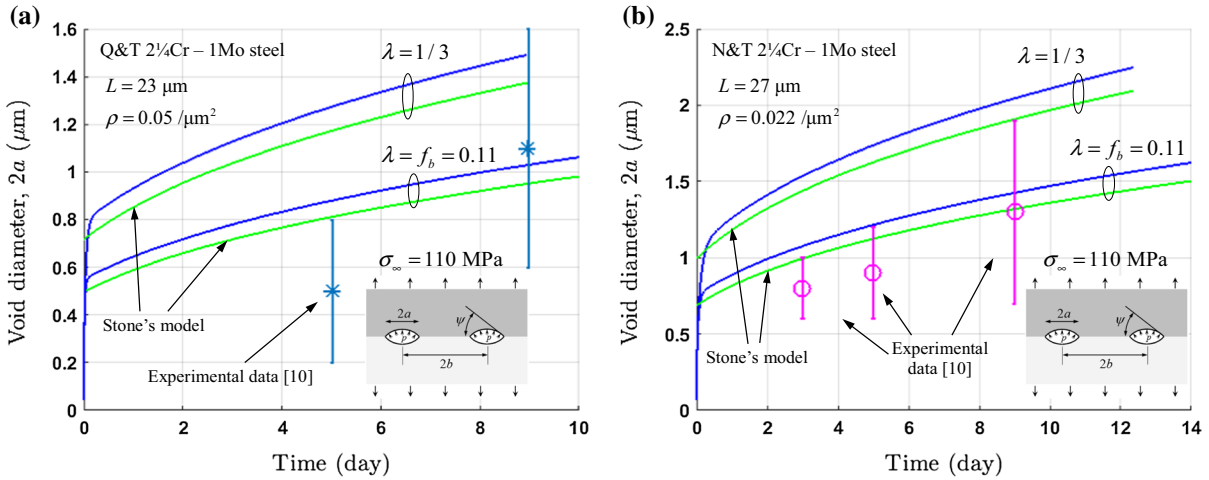

Fig. 12 Effect of λ, the fraction of the grain that accommodates void growth, on the void growth predictions of the present mode and Stone's model for **a** quenched and tempered 21/4Cr–1Mo steel and **b** normalized and tempered 21/4Cr–1Mo steel in 13.8 MPa H_2 gas, 600 °C environment, and 110 MPa external stress σ_∞. The grain size is L and the bubble number density on cavitated GBs ρ is shown in the figures for each material. The cavitated GB area fraction was assumed $f_b = 0.11$, the initial void diameter $2a_0 = 0.02b = 0.0447$ μm with $2b$ being the bubble spacing, and the calculated bubble pressure was $p = 94.3$ MPa. The experimental data of Stone are also superposed (Stone 1984)

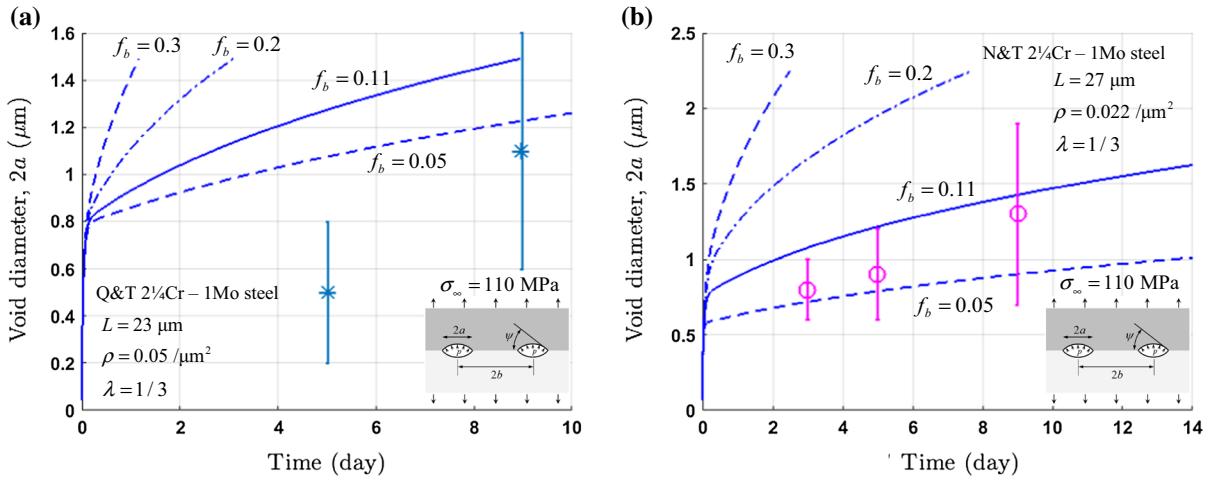

Fig. 13 Effect of cavitated GB area fraction f_b on the present model's predictions of constrained void growth for **a** quenched and tempered 21/4Cr–1Mo steel and **b** normalized and tempered 21/4Cr–1Mo steel in 13.8 MPa H_2 gas, 600 °C environment, and 110 MPa external stress σ_∞. The grain size is L, the bubble number density on cavitated GBs ρ, and the fraction of the grain that accommodates the void growth λ are showed on the figures. The initial void diameter was assumed $2a_0 = 0.02b = 0.0447\,\mu$m with $2b$ being the bubble spacing, and the calculated bubble pressure was $p = 94.3$ MPa. The experimental data identified with error bars are also superposed for comparison (Stone 1984)

$\lambda = f_b$ in his model. Figure 12a, b show the effect of this assumption on the void growth results respectively for Q&T and N&T 21/4Cr–1Mo steels. Superposed on the figure are the void diameter results for $\lambda = 1/3$ (Figs. 4a, 5a). Although the predictions of the present model and Stone's model with $\lambda = f_b$ are closer to the experimental data, we believe that the assumption $\lambda = f_b$ is not accurate and hence it should not be adopted.

We also investigated the effect of the area fraction of the cavitated grains f_b on void growth under external load. As shown in Fig. 13, increasing f_b increases the void growth rate for both Q&T and N&T 21/4Cr–1Mo steel. However, the effect of an increasing f_b on N&T steel, Fig. 13b, is more pronounced as it also affects the initial stage of the constrained void growth process as well as the growth rate. This is attributed to the smaller value of the bubble number density on cavitated GBs ρ in the N&T steel in comparison to that in the Q&T steel which results in a larger bubble spacing $2b$.

References

API RP 941 (2016) Steels for hydrogen service at elevated temperatures and pressures in petroleum refineries and petrochemical plants, 8th edn. American Petroleum Institute Recomended Practice 941, API Publishing Services

API TR 941 (2008) The technical basis document for API RP 941. American Petroleum Institute Technical Report 941, API Publishing Services

Chao B-L (1987) Kinetics and mechanisms of hydrogen attack in 2.25 Cr-1 Mo steel. PhD Dissertation, University of California, Santa Barbara

Chuang TJ, Kagawa KI, Rice JR, Sills LB (1979) Non-equilibrium models for diffusive cavitation of grain interfaces. Acta Metall 27:265–284. https://doi.org/10.1016/0001-6160(79)90021-X

Darken LS, Gurry RW (1953) Physical chemistry of metals. McGraw Hill, New York

Davis JR (ed) (1997) ASM specialty handbook: heat-resistant materials. ASM International, Materials Park

Erwin WE (1982) Mechanisms of hydrogen attack in 21/4Cr–1Mo reactor steel. In: 47th midyear meeting of the API. API, New York, pp 120–134

Frost HJ, Ashby MF (1982) Deformation-mechanism maps, the plasticity and creep of metals and ceramics. Pergamon Press, Oxford

Grabke HJ, Martin E (1973) Kinetics and thermodynamics of the carburization and decarburization of α-iron in CH_4-H_2 mixtures. Arch fuer das Eisenhuettenwes 44:837–842

Klueh RL (1980) Creep and rupture behavior of a bainitic 2 1/4 Cr–1 Mo steel. Int J Press Vessel Pip 8:165–185. https://doi.org/10.1016/0308-0161(80)90023-X

Needleman A, Rice JR (1980) Plastic creep flow effects in the diffusive cavitation of grain boundaries. Acta Metall 28:1315–1332. https://doi.org/10.1016/0001-6160(80)90001-2

Odette GR, Vagarali SS (1982) An equation-of-state for methane for modeling hydrogen attack in ferritic steels. Metall Trans A 13:299–303. https://doi.org/10.1007/BF02643320

Parthasarathy TA (1985a) Mechanisms of hydrogen attack of carbon and 21/4Cr–1Mo steels. Acta Metall 33:1673–1681

Parthasarathy TA, Lopez HF, Shewmon PG (1985b) Hydrogen attack kinetics of 2.25 Cr–1 Mo steel weld metals. Metall Trans A 16:1143–1149. https://doi.org/10.1007/BF02811683

Sagues AA, Okray Hall B, Wiederslch H (1978) On the mechanisms of hydrogen attack. Scr Metall 12:319–326

Schlogl SM, Svoboda J, Van der Giessen E (2001) Evolution of the methane pressure in a standard 2.25Cr–1Mo steel during hydrogen attack. Acta Mater 49:2227–2238. https://doi.org/10.1016/S1359-6454(01)00132-X

Schlogl SM, Van der Giessen E (2001) Micromechanics of high temperature hydrogen attack. Int J Numer Methods Eng 52:559–567. https://doi.org/10.1002/nme.299

Schlogl SM, Van der Giessen E (2002) Computational model for carbon diffusion and methane formation in a ferritic steel during hydrogen attack. Scr Mater 46:431–436. https://doi.org/10.1016/S1359-6462(02)00008-8

Schlogl SM, Van Leeuwen Y, Van der Giessen E (2000) On methane generation and decarburization in low-alloy Cr–Mo steels during hydrogen attack. Metall Mater Trans A 31:125–137. https://doi.org/10.1007/s11661-000-0059-5

Sham TL, Needleman A (1983) Effects of triaxial stressing on creep cavitation of grain boundaries. Acta Metall 31:919–926. https://doi.org/10.1016/0001-6160(83)90120-7

Shewmon PG (1976) Hydrogen attack of carbon steel. Metall Trans A 7:279–286. https://doi.org/10.1007/BF02644468

Shewmon PG (1987) Synergism between creep ductility and grain boundary bubbles. Acta Metall 35:1317–1324. https://doi.org/10.1016/0001-6160(87)90013-7

Shewmon PG, Yu ZS (1982) Hydrogen attack kinetics in 21/4Cr–1Mo pressure vessel steel. In: Degradation of materials symposium, ACS-AIME Meeting, Louisville, pp 85–92

Shih H-M, Johnson RR (1982) A model calculation of the Nelson curves for hydrogen attack. Acta Metall 30:537–545. https://doi.org/10.1016/0001-6160(82)90234-6

Stone DS (1984) Hydrogen attack in 2.25 Cr–1.0 Mo steels. PhD Dissertation, Cornell University

Sundararajan G, Shewmon PG (1981) The kinetics of hydrogen attack of steels. Metall Trans A 12:1761–1775. https://doi.org/10.1007/BF02643758

Vagarali SS, Odette GR (1981) A model for the growth of hydrogen attack cavities in carbon steels. Metall Trans A 12:2071–2082. https://doi.org/10.1007/BF02644177

Van der Burg MWD, Van der Giessen E (1996a) Non-uniform hydrogen attack cavitation and the role of interaction with creep. Mater Sci Eng A 220:200–214. https://doi.org/10.1016/S0921-5093(96)10465-2

Van der Burg MWD, Van der Giessen E (1996b) Hydrogen attach in creeping polycrystals due to cavitation on grain boundaries. In: Thompson AW, Moody NR (eds) Hydrogen effects in materials. TMS, Pittsburgh, pp 313–322

Van der Burg MWD, Van der Giessen E (1997) A continuum damage relation for hydrogen attack cavitation. Acta Mater 45:3047–3057. https://doi.org/10.1016/S1359-6454(96)00382-5

Van der Burg MWD, Van der Giessen E, Brouwer RC (1996) Investigation of hydrogen attack in 2.25 Cr–1Mo steels with a high-triaxiality void growth model. Acta Mater 44:505–518

Van der Giessen E, Van der Burg MWD, Needleman A, Tvergaard V (1995) Void growth due to creep and grain boundary at high triaxialities. J Mech Phys Solids 43:123–165

Yu ZS, Shewmon PG (1981) Hydrogen attack of 21/4 Cr–1 Mo Pressure vessel steel. In: Environmental degradation of engineering materials in hydrogen, Blacksburg, pp 253–260